ISSN 1027-5495. Functional Materials, 33, No.3 (2026), p. 604-614
doi:http://dx.doi.org/10.15407/fm33.03.604 © 2026 — SSI "Institute for Single Crystals"
This is an open access article under the CC BY-NC-ND license (http://creativecommons.org/licenses/by-nc-nd/4.0/).

Designing the silica-coated hexagonal gold nanoparticles-based localized surface plasmon resonance sensor for albumin detection

Lilik Hasanah[1,*], Silva Nurfasha[1], Budi Mulyanti[2], Yanurita Dwi Hapsari[3], Heni Rusnayati[4], Ahmad Aminudin[1], Ida Hamidah[5], Siti Kudnie Sahari[6], Chandra Wulandari[1,*]

[1]Physics Study Program, Universitas Pendidikan Indonesia, Jl. Dr. Setiabudhi 229 Bandung 40154, Jawa Barat, Indonesia
[2]Electrical Engineering Education Study Program, Universitas Pendidikan Indonesia, Jl. Dr. Setiabudhi 229 Bandung 40154, Jawa Barat, Indonesia
[3]Department of Physics, Institut Teknologi Sepuluh Nopember (ITS), Surabaya 60111, Indonesia
[4]Physics Education Study Program, Universitas Pendidikan Indonesia, Jl. Dr. Setiabudhi 229 Bandung 40154, Jawa Barat, Indonesia
[5]Mechanical Engineering Education Study Program, Universitas Pendidikan Indonesia, Jl. Dr. Setiabudhi 229 Bandung 40154, Jawa Barat, Indonesia
[6]Faculty of Engineering, Universiti Malaysia Sarawak, 94300 UNIMAS, Kota Samarahan, Sarawak, Malaysia
*Email corresponding: lilikhasanah@upi.edu, chandra.wdr@upi.ed

Received October 19, 2025, aproved May 10, 2026

Localized surface plasmon resonance (LSPR) has been demonstrated as a promising detection technique due to their high sensitivity as reported in numerous studies. LSPR enables direct interaction between gold nanoparticles, which act as transducers, with the target in the surrounding environment. Therefore, the development of nanoparticles is a key approach to enhancing the sensitivity of LSPR sensors. In this study, we propose silica-coated hexagonal gold nanoparticles (Si@hexaAu), which are geometrically optimized using Finite-Difference Time-Domain simulation methods. The silica coating is applied to modify the refractive index sensitivity of gold nanoparticles while minimizing nanoparticle agglomeration. We optimize the nanoparticles by varying the height (h) and lateral size (l) of the hexagonal structure, and thickness (t) of silica coating. The highest enhancement in refractive index sensitivity is achieved with Si@hexaAu with h = 30 nm, l = 100 nm, and t = 9 nm. The albumin detection performance is simulated by applying the refractive index of various albumin concentrations to both bare hexaAu and Si@hexaAu. The sensitivity and limit-of-detection of Si@AuNPs of 3.28 nm/mM and 0.62 mM, are superior to those of bare hexaAu of 2.52 nm/mM and 0.79 mM, respectively. This study successfully demonstrates the importance of geometry optimization and the advantages of coating modifications for nanoparticles in LSPR sensors.

Keywords: localized-surface plasmon resonance, hexagonal gold nanoparticles, silica-coating, geometry optimization, finite-difference time-domain.

Проектування датчика локалізованого поверхневого плазмонного резонансу на основі гексагональних наночастинок золота з кремнеземним покриттям для виявлення альбуміну. *Lilik Hasanah, Silva Nurfasha, Budi Mulyanti, Yanurita Dwi Hapsari, Heni Rusnayati, Ahmad Aminudin, Ida Hamidah, Siti Kudnie Sahari, Chandra Wulandar*

Локалізований поверхневий плазмонний резонанс (LSPR) продемонстрував себе як перспективний метод виявлення завдяки своїй високій чутливості, про що повідомляється в численних дослідженнях. LSPR забезпечує пряму взаємодію між наночастинками золота як перетворювачами з мішенню в навколишньому середовищі. Тому розробка наночастинок є ключовим підходом до підвищення чутливості датчиків LSPR. У цьому дослідженні ми пропонуємо покриті кремнеземом гексагональні наночастинки золота (Si@hexaAu), які геометрично оптимізовані за допомогою методів моделювання в часовій області з кінцевими різницями. Кремнеземне покриття наноситься для зміни чутливості показника заломлення золотих наночастинок, мінімізуючи агломерацію наночастинок. Ми оптимізуємо наночастинки, змінюючи висоту (h) та поперечний розмір (l) гексагональної структури, а також товщину (t) кремнеземного покриття. Найвище підвищення чутливості показника заломлення досягнуто з Si@hexaAu з h = 30 нм, l = 100 нм та t = 9 нм. Продуктивність виявлення альбуміну моделюється шляхом застосування показника заломлення різних концентрацій альбуміну як до чистого hexaAu, так і до Si@hexaAu. Чутливість та межа виявлення Si@AuNPs, що становлять 3,28 нм/мМ та 0,62 мМ, перевершують аналогічні показники чистого hexaAu, що становлять 2,52 нм/мМ та 0,79 мМ відповідно. Це дослідження успішно демонструє важливість оптимізації геометрії та переваги модифікації покриття для наночастинок у LSPR-сенсорах.

1. Introduction

Albumin is the most abundant plasma protein synthesized by the liver and plays an essential role in physiological homeostasis, including maintaining colloidal osmotic pressure and binding/transporting a wide range of endogenous and exogenous molecules in the bloodstream [1]. Serum albumin is routinely measured in clinical practice and is clinically relevant in kidney-related disorders: glomerular diseases with substantial protein loss can lead to hypoalbuminemia, and lower serum albumin has also been associated with poorer outcomes in advanced chronic kidney disease (CKD) [2], [3]. Given that CKD is a major global health burden affecting more than 10% of the population worldwide, developing reliable and sensitive approaches for serum albumin detection and monitoring is important to support kidney disease assessment and patient management [4]. Various conventional methods have been used to monitor serum and urinary albumin levels, including salt fractionation, electrophoresis, light scattering, chemiluminescence, and high-performance liquid chromatography [5], [6]. However, these methods are limited by complex pretreatment procedures, long analysis times, poor sensitivity, and high costs [7], [8]. Therefore, the development of advanced albumin detection techniques is important to improve the diagnosis and management of kidney disease.

Localized surface plasmon resonance (LSPR) is a unique optical property exhibited by gold nanoparticles that refers to the collective oscillation of electrons in the conduction band of gold nanoparticles which resonate with a specific wavelength of incident light [9]. LSPR has been utilized as the main device principle or the support to enhance device performance. It has been reported in some applications including, sensing, imaging [10], photocatalysis [11], solar cells [12], and therapeutic [13]. LSPR-based sensing becomes the most explored application due to its high sensitivity to the change the surrounding environment of the metal nanoparticles. In LSPR-based sensing, analyte molecules directly interact with the metal nanoparticles and change the dielectric constant around them thereby modifying the resonance wavelength. The LSPR-based sensing demonstrates excellent results in the detection of proteins, molecules, deoxyribonucleic acid, polymers, and other chemical and biological substances [14], [15]. LSPR sensors rely on the use of a small and defined sensing surface area, which is advantageous in the detection of small molecules, low-concentration samples, and limited samples [16]. The properties of metal nanoparticles are becoming a key aspect in the development of LSPR. Therefore, the control of the shape, size, and composition of the nanoparticles is the main strategy to obtain the higher sensitivity of LSPR sensors. Among the noble metal nanoparticles, gold- and silver-nanoparticles, have always demonstrated the most satisfying sensitivity, since their LSPR absorption and scattering occur within the visible light spectrum [17].

The optimization of the shape and size of gold nanoparticles have been reported with different techniques and approaches. In one of the studies, the size of star-shaped gold nanoparticles varied with a size range of approximately 116.4 ± 26.92 nm. This star shape was chosen for its functional properties and ability to amplify signals, making it suitable for biomedical applications [18]. Another study investigated the size of rod-shaped gold nanoparticles with an aspect ratio ranging from 4 to 7. This rod shape was chosen due to its ability to significantly modify the LSPR resonance wavelength based on the aspect ratio and the dielectric constant of the surrounding medium, making it suitable for applications in the fields of biomedicine and photonics [19]. A number of sources have chosen to vary the size of hexagonal-shaped gold nanoparticles with a range of sizes due to their ability to generate strong LSPR, which can enhance the electromagnetic field around the nanoparticles [17]. Compared to triangular gold nanoparticles and nanobipyramids, hexagonal gold nanoparticles (hexaAu) exhibit higher sensitivity to changes in refractive index [20]. HexaAu have unusually strong localized electromagnetic fields at their vertices and corners. They also exhibit low plasmon attenuation due to their low surface roughness [20]. Studies on Au nanoplates have shown high refractive-index sensitivity to the surrounding dielectric environment, where the LSPR peak redshifts as the edge length increases and the LSPR intensity enhancing as the thickness increases [21]. These observations indicate that hexaAu can be optimized by controlling the height and lateral size, since these geometric parameters effectively influence the optical properties of LSPR.

The aggregation of gold nanoparticles also becomes a challenge to overcome because it limits the application of LSPR in biological environments. Coating the gold nanoparticles with a stabilizing agent such as a thiol-based compound, surfactants, and biomolecules is a promising way [22]. However, they generally could easily degrade over time and thus can cause contamination and interference. Silica coating is a well-known and robust technique to enhance the metal nanoparticle stability and biocompatibility [23]. Silica-coated gold nanoparticles have a higher refractive index sensitivity of 30% compared to surfactant cetyltrimethylammonium bromide-coated gold nanoparticles [24]. In addition, silica coating does not produce cytotoxicity which can be harmful for medical application [25]. These findings indicate that silica modification can suppress aggregation and improve biological stability while enhancing the LSPR sensitivity of gold nanoparticles. However, overly thick silica layer can decouple binding events from the plasmonic surface and weaken the measurable LSPR shift. Conversely, ultrathin silica can preserve strong field analyte coupling while still providing protection and improved sensing performance [26], [27]. Therefore, the silica coating thickness must be tuned to obtain the optimal balance between nanoparticle stability and maximal LSPR sensitivity for reliable biosensing performance.

In this study, silica-coated hexagonal gold nanoparticles (Si@hexaAu) were designed for LSPR-based albumin detection using finite-difference time-domain (FDTD) simulations. The geometry of the hexagonal gold nanoparticles was optimized by tuning the lateral size and height to enhance plasmonic sensitivity. In addition, silica coating modification was investigated by systematically varying the silica thickness to balance nanoparticle stability and near-field coupling. To the best of our knowledge, no prior study has systematically examined the dependence of LSPR sensing performance on the geometric design of hexagonal gold nanoparticles, particularly in the presence of a tunable silica coating. Finally, the optimized Si@hexaAu design was applied to albumin detection by tracking refractive-index–induced LSPR changes within the same simulated platform. The results demonstrate the nanoparticle performance not only in terms of optical response (e.g., absorption characteristics), but also in terms of key sensing metrics, including sensitivity and limit-of-detection.

2. Materials and Methods

The Si@hexaAu developed in this study consisted of hexagonal gold nanoparticles as the core conformally coated with a thin silica shell, as illustrated in Figure 1. Before evaluating the silica coating effect, the influence of the height (h) and lateral size (l) of the core of uncoated hexagonal gold nanoparticles was first investigated. The h:l ratio was fixed at 3:8 to preserve the nanoplate-like hexagonal geometry during size scaling, allowing the size effect on the LSPR response to be evaluated without additional shape variation. The use of a hexagonal nanoplate model was guided

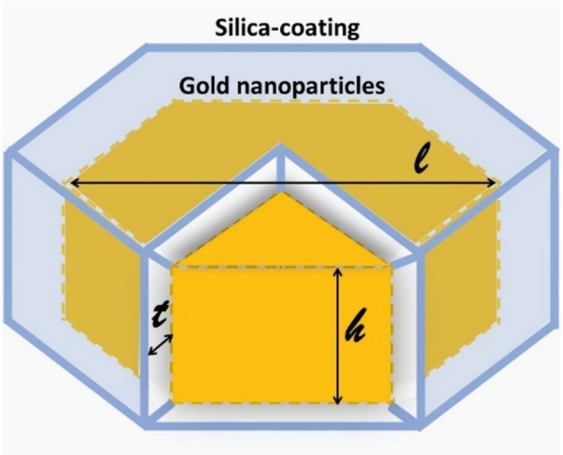

Figure 1. Schematic illustration of hexagonal Si@hexaAu. The illustration shows the thin silica layer coating the hexagonal AuNPs as the core. The arrow pointed out the parameters optimized in this study.

by previous reports showing that hexagonal gold nanoplates exhibit strong plasmonic responses and high potential for LSPR-based sensing [17]. The variation of h is 15–90 nm and the l is 40–240 nm. In addition, we varied the thickness of the silica coating (t: 1 – 10 nm) since the inappropriate coating on the gold surface could weaken the evanescent field of surface plasmon [28].

The optimization of nanoparticle design was done using finite-difference time-domain (FDTD)-based simulation in the system assembly and simulation software. This approach allows us to build the nanoparticle design with controlled parameters visually. The FDTD numerically solves Maxwell's equations in time on a Yi grid. on a Yee grid [29]. The computational domain was terminated using a perfectly matched layer (PML) boundary conditions which simulate open space and suppress unphysical reflections [30]. A linearly polarized broadband plane-wave source (e.g., TSFS source) covering 300–900 nm was used to excite the nanoparticle. The incident light was directed normal to the hexagonal face of the particle, corresponding to propagation along the z-axis and perpendicular to the xy-plane as shown in Figure 1. The optical response was recorded using frequency-domain power monitors placed around the nanostructure. The absorption spectrum was obtained from the calculated absorbed power, and the LSPR wavelength was determined from the maximum peak position of the absorption spectrum.

The sensing performance was evaluated by performing simulations at different refractive indices. The change in the refractive index represents the change in analyte concentration, thus, we use the refractive index appropriate for various albumin concentrations. Human serum albumin (HSA) is homologous to bovine serum albumin (BSA). BSA in the medical field is considered more efficient because it is easily obtained and much cheaper [31]. Therefore, in this study, we use the refractive index of BSA as listed in Table 1 [32]. In the FDTD simulation system, this refractive index was applied as a background index of the simulated Si@hexaAu.

Table 1. Refractive index of bovine serum albumin (BSA) at different concentrations [33]. This concentration was used as a background index in the FDTD simulation to represent the detection of albumin by the proposed Si@hexaAu.

Concentration (mM)	Refractive Index
0.39	1.33
0.67	1.34
1.79	1.35
2.97	1.36
4.09	1.37
4.83	1.38

In the simulation system, the Si@hexaAu were modeled as shown by the schematic illustration in Figure 1 and placed inside the FDTD simulation region equipped with the simulated light source and monitor. The used source illuminated the nanoparticles with a plane wave electromagnetic field propagating from the top surface of the hexagon. Around the nanoparticles, the monitor records the absorption obtained by the nanoparticle different wavelengths. This data was similar to the LSPR experimental study, that used UV-visible analysis to determine the wavelength-absorption dependence. The absorption peak will be shifted when the background index of the simulation changes. Therefore, the detection performance of LSPR sensors is determined by the shift of the peaks along the wavelength axes ($\Delta\lambda$) depending on the change in analyte concentration (ΔC) or directly the refractive index (ΔRI) [15]. The sensitivity (S) and limit-of-detection (LOD) of LSPR are calculated by Equations 1 and 2, respectively.

$$S = \frac{\Delta\lambda_{LSPR}}{\Delta RI} \text{ or } \frac{\Delta\lambda_{LSPR}}{\Delta C} \quad (1)$$

$$LOD = \frac{3.3\sigma}{m} \quad (2)$$

where σ and m are, respectively, the standard deviation and slope obtained from the linear fitting [28], [34]. The 3.3 value is a multiplier used

to estimate the lowest concentration of an analyte that can be reliably distinguished from the blank, corresponding to a 95% confidence level.

3. Results and Discussion

This study is aimed to observe the influence of geometric parameters of the hexagonal structure divided in three aspects: the size of particles, the lateral size, and the thickness of silica-coating. Firstly, the particle size (h and l simultaneously) and lateral size (l) were optimized on the bare hexaAu. Afterward, the optimal geometric parameters were used to optimize silica-coating thickness on the hexaAu. Hexagonal nanostructures can be classified into different geometries depending on their height-to-lateral size (h:l) ratio. Structures with relatively small height are commonly considered nanoplate-like particles, whereas structures with larger height may resemble nanocylinders or nanowires. Therefore, this study was limited to hexagonal nanoplate-like nanoparticles. In this work, particle size refers to the simultaneous scaling of the height (h) and lateral size (l) while maintaining a constant h:l ratio of 3:8. By keeping this ratio fixed, the overall particle shape was preserved, allowing the effect of size on the LSPR response to be evaluated without additional shape variation.

Figure 2(a) shows the LSPR absorption spectra of hexaAu particles of different size (RI = 1.33), illustrating that the absorption spectra change significantly for each variation in particle size. The hexaAu particles generally exhibit dual LSPR resonances due to their highly anisotropic, plate-like geometry, which supports plasmon oscillations along two distinct axes. The short axis corresponds to out-of-plane or thickness side, and the long axis corresponds to in-plane or lateral side. These modes are commonly denoted as transverse and longitudinal resonances, respectively [35], [36]. Here, the simulated hexaAu particles show two LSPR peaks at approximately 600 nm and 700 nm, which agrees well with the dual-band LSPR behavior reported in experimental LSPR systems. Morsin et al. synthesized Au nanoplates on a quartz substrate and observed two LSPR bands: a transverse band at 545 nm and a longitudinal band at 710 nm. [36]. In addition, experimental UV-Vis studies on thin Au nanoplates exhibited a peak near 580 nm with longer-wavelength band around 685 nm [35]. These findings highlight that the exact peak positions depend on the particle geometry and the dielectric environment. In the present simulation, the LSPR spectra did not show a simple monotonic shift with increasing particle size. However, size-dependent changes in peak broadening, mode separation, and the emergence of additional resonances were observed. In particular, the hexaAu nanoplates with h = 45 nm and l = 120 nm exhibited an additional absorption peak at approximately 570 nm. This peak can be assigned to an additional plasmon mode, most likely related to the transverse/out-of-plane resonance or a higher-order multipolar mode of the hexagonal nanoplate-like structure. Although the h:l ratio was maintained, the increase in absolute particle dimensions can alter the field distribution and spectral separation between different plasmon modes, making this additional resonance more pronounced at this specific size [37], [38], [39]. Smaller metal nanoparticles typically experience surface scattering, a mechanism that couples the surface plasmon collective mode with non-harmonic single electron-hole pair excitations, thereby damping the LSPR signal [40], [41], [42]. This phenomenon is also observed in silver nanoparticles with diameters smaller than 25 nm [42], [43]. Meanwhile, the larger particle size results in broad and indistinct peaks because of the multipole resonance modes and dynamic depolarization [44], [45].

The optimal LSPR peaks were observed from the hexaAu nanoplates with h = 30 nm and l = 80 nm which showed a sharp peak at 621.05 nm. To verify these results, the size variation was then simulated in the different background index to predict their potential for sensing application. The results of this study are presented in Table 2. Figure 2(b) shows the most distinct shifting produced by hexaAu nanoplates with h = 30 nm and l = 80 nm, where the refractive index changes from 1.33 to 1.34 peaks shifted from 621.13 nm to 623.8 nm. Their total shifting of $\Delta\lambda$ = 2.67 nm turned out to be more significant compared to other options, which confirmed the optimality of the size parameters. The size was then used in the study of lateral size variation while the height was kept constant by h = 30 nm.

By varying the lateral size, we aim to get the larger shifting towards the refractive index changes. Figure 3(a) shows that as the lateral size increased from 20 nm to 120 nm (RI = 1.33), the LSPR peaks were red-shifted, getting higher, and broader. Therefore, the optimal parameters will be generated by the value in the

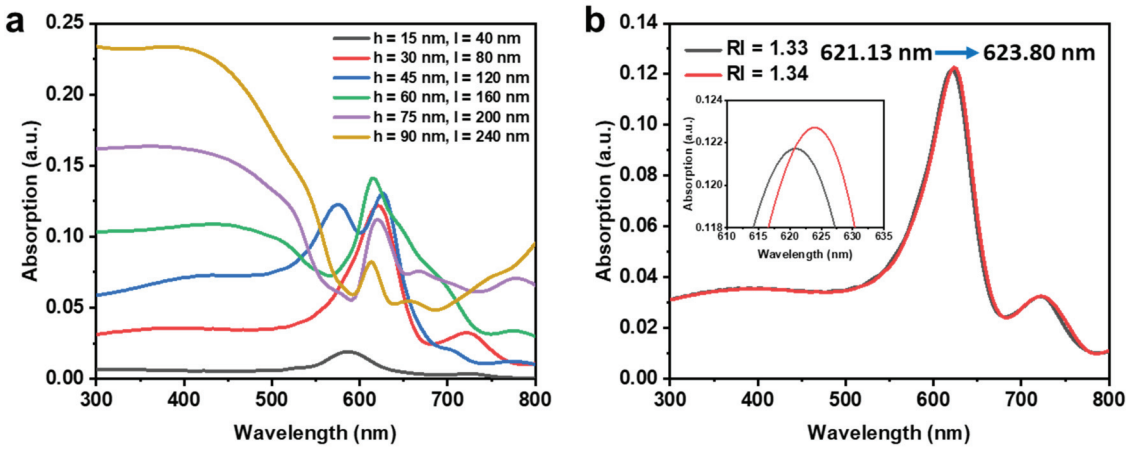

Figure 2. Effect of size of hexaAu nanoplates on the LSPR absorption properties (*h*:*l ratio* 3:8). (a) Absorption spectra resulting from each size variation at a refractive index of 1.33, (b) Absorption peak shifting due to a change in background refractive index from 1.33 to 1.34 (h = 30 nm, l = 80 nm); insets show magnified peaks for clear shifting.

Table 2. Absorption peak shift due to a change in background refractive index from 1.33 to 1.34 for each size variation. The table listed the absorption peak position for each refractive index and their differences ($\Delta\lambda_{LSPR}$)

h, l (nm)	λ_{LSPR} (RI = 1.33)	λ_{LSPR} (RI = 1.34)	$\Delta\lambda_{LSPR}$
15, 40	586.17	587.37	1.2
30, 80	621.13	623.8	2.67
45, 120	626.38	628.11	1.73
60, 160	615.27	617.28	2.01
75, 200	621.05	623.4	2.35
90, 240	613	614	1

middle of the variation range. In the previous discussion, we obtained the l = 80 nm which gave a sharp peak with a refractive index shift from 1.33 to 1.34 at 2.67 nm. With l = 100 nm, the shift was slightly further from 644.97 nm to 647.8 nm ($\Delta\lambda$ = 2.87 nm). Since the detection activity of LSPR was measured by this shift, even this small increase is valuable for obtaining better LSPR sensing performance. The detailed wavelength changes for each lateral size variation is listed Table 3.

In experimental systems, the optical response of gold nanoparticles is often affected by agglomeration, which can modify the absorbance signal because of non-uniform light–nanoparticle interactions. The measured LSPR signal represents the collective contribution of the particle population dispersed in the solution [46]. Among several strategies to suppress agglomeration, silica coating is widely used because it can improve nanoparticle stability, reduce direct particle–particle contact, and provide a chemically compatible surface for further target recognition without introducing substantial contamination [23]. As shown in Figure 1, the LSPR properties of Si@hexaAu were simulated by varying the silica shell thickness. The silica shell can affect the plasmonic response through two competing mechanisms by increasing the local dielectric environment around the hexaAu core, which generally induces a red-shift, and an increase in the interparticle distance, which weakens plasmon coupling and may cause a blue-shift [47]. Figure 4 shows that, within the thickness range of 1–7 nm, the LSPR peak shifted to longer wavelengths and became broader with increasing silica thickness. This behavior is attributed to the increased effective refractive index around the hexaAu core and is consistent with previous reports that used the LSPR redshift as an indicator of silica coating formation [48].

For thicker silica shells of 8–10 nm, the spectral trend became non-monotonic. The absorp-

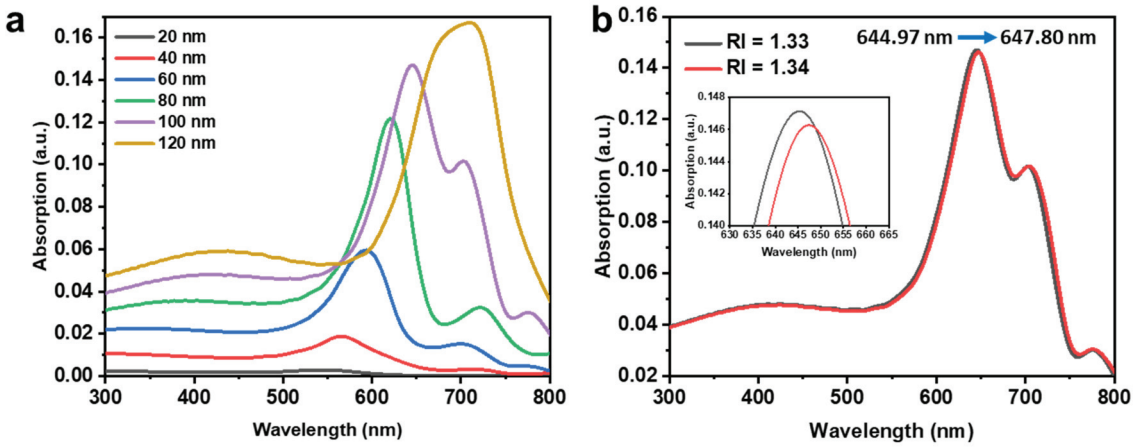

Figure 3. Effect of lateral size (*l*) of hexaAu on the LSPR absorption properties (constant h = 30 nm). (a) Absorption spectra resulting from different lateral size variation at refractive index of 1.33, (b) Absorption peak shift due to the change of background refractive index from 1.33 to 1.34 (l = 100 nm); insets show magnified peaks for clear shifting.

Table 3. Absorption peak shift due to a change in the background refractive index from 1.33 to 1.34 for each lateral size (l) variation (with constant h = 30 nm). The table listed the absorption peak position for each refractive index and their differences ($\Delta\lambda_{LSPR}$)

l (nm)	λ_{LSPR} (RI = 1.33)	λ_{LSPR} (RI = 1.34)	$\Delta\lambda_{LSPR}$
20	542.31	543.38	1.07
40	565.5	566.6	1.1
60	593.4	594.7	1.3
80	621.13	623.8	2.67
100	644.97	647.8	2.83
120	710.6	712.9	2.3

tion peak shifted from approximately 1100 nm to 1000 nm for the 8 and 10 nm shells, while the 9 nm shell showed a shorter-wavelength response at approximately 750 nm. This result indicates that the LSPR behavior in this narrow thickness range is not controlled solely by the dielectric effect of silica. Instead, this behavior may reflect a non-linear balance between dielectric screening, reduced interparticle plasmon coupling, local field redistribution, and geometry-dependent plasmon confinement in the hexagonal structure. The dielectric environment surrounding gold nanoparticles strongly affects their LSPR response, while the silica shell can also act as a spacer that increases the separation between neighbouring hexaAu cores and weakens plasmon coupling [49], [50]. In addition, the plasmonic response of anisotropic or faceted gold nanostructures is sensitive to particle geometry, edge curvature, and local field distribution [39], [49], [51]. Therefore, the "9 nm" result should be interpreted with caution as a model-predicted non-monotonic response within the current simulation resolution, rather than as a definitive optimum caused only by the silica shell thickness. A more accurate scanning range of 8–10 nm would be useful for future optimization, since the FDTD accuracy in plasmonic nanoparticle systems depends on mesh refinement and convergence testing [52].

The simulation successfully demonstrates the optimum parameters of Si@hexaAu, with dimensions h = 30 nm, l = 100 nm, and t = 9 nm. The detection of albumin was simulated by changing the background index around the nanoparticles to imitate the condition of LSPR samples. In a real LSPR-sensor sample, the target object was dissolved in the nanoparticle solution thus changing the refractive index of the entire solution. A refractive index of 1.33 to 1.38 was used, with each value corresponding to a different albumin concentration, as shown in Table 1. In this discussion, we compared the detection performance of bare hexaAu and Si@hexaAu. Figure 5(a) shows the LSPR absorption spectrum from bare hexaAu

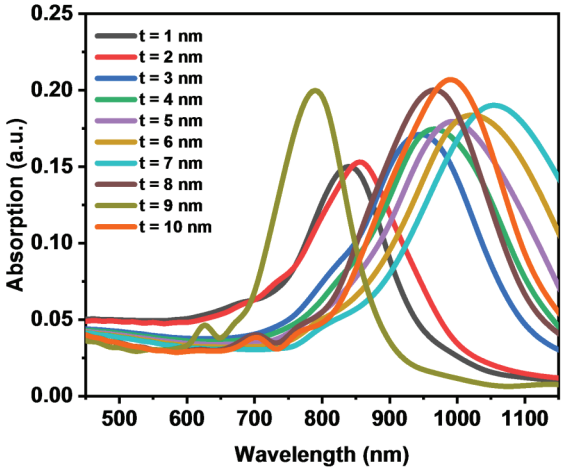

Figure 4. Effect of silica-coating thickness of Si@hexaAu on the LSPR absorption properties. The best results for hexaAu were obtained at h = 30 nm and l = 100 nm.

that shifted to a higher wavelength as the refractive index increased. A similar pattern was provided by the absorption spectra of Si@hexaAu (Figure 5(c)) and this agrees with the relation of dielectric constant with wavelength. Figures 5(b) and 5(d) show more clearly the difference between bare hexaAu and Si@hexaAu. By changing the x-axis to the albumin concentration and plotting the peak position in the y-axis, we obtained the linear regression of this relation. The gradient depicts the sensitivity of sensors because it quantifies the peak shift caused by changes in the concentration of the target substance. Both plots against concentration and refractive index (in the inset) show a higher sensitivity from the Si@hexaAu of 3.28 nm/mM (R^2 = 0.979) compared to bare AuNPs with a sensitivity of 2.52 nm/mM (R^2 = 0.967). The detection limit (LOD) was calculated based on Equation 2 resulting in the LOD of bare hexaAu being 0.79 mM while Si@hexaAu was 0.62 mM. The sensitivity and LOD values confirmed that Si@hexaAu provides superior sensor performance for albumin. The refractive index sensitivity obtained from the linear regression (in the inset) was used to compare our results to the reported gold nanparticle LSPR sensor. The sensitivity of 312.01 nm/RIU was superior compared to numerous studies and potential for development in the future [53], [54]. Although this study focused on refractive index changes caused solely by albumin, we acknowledge that real biological fluids contain numerous other components that may also influence the refractive index. These components were not considered in this simulation. However, the sensitivity to refractive index changes is sufficiently representative to demonstrate the general applicability of the proposed LSPR sensor for albumin detection in various media. This is because the refractive index change caused by albumin concentration remains proportional, even when the base refractive index changes depending on the dissolved medium [55].

4. Conclusion

This work presents a simple FDTD-simulated design strategy for LSPR nanoparticles based on hexaAu and their silica-coated counterparts (Si@hexaAu). We simulated the LSPR response of hexaAu by systematically varying the height (h) and lateral size (l) and evaluating the peak shift in the surrounding refractive index range of n = 1.33–1.34. The optimized hexagonal geometry (h = 30 nm, l = 100 nm) provided a peak shift of 2.83 nm and made it possible to achieve a refractive index sensitivity of 312.01 nm/RIU. We then investigated silica-shell thicknesses (t = 1–10 nm) and observed two regimes, where thin shells primarily modify the local dielectric environment, whereas thicker shells increasingly screen the plasmonic near field, altering the LSPR response. An optimal silica thickness of t = 9 nm provided the best overall sensing performance, improving the apparent concentration sensitivity (S = 3.28 nm mM^{-1}) and the corresponding LOD (0.62 mM) compared with bare hexaAu. Since the concentration-to-shift conversion is based on the refractive-index data reported for albumin in distilled water, absolute peak positions and concentration mapping should be recalibrated for serum or plasma matrices under actual application conditions. Although real matrices were not explicitly simulated in this work, the results clearly demonstrate the significance of systematically optimizing hexagonal Si@hexaAu to achieve enhanced LSPR sensing performance and improved detection capability. A key future challenge is to incorporate clinically relevant matrices and surface-binding effects through serum-based calibration, enabling more accurate translation of peak shifts into clinically meaningful albumin concentrations and validation under realistic sample conditions.

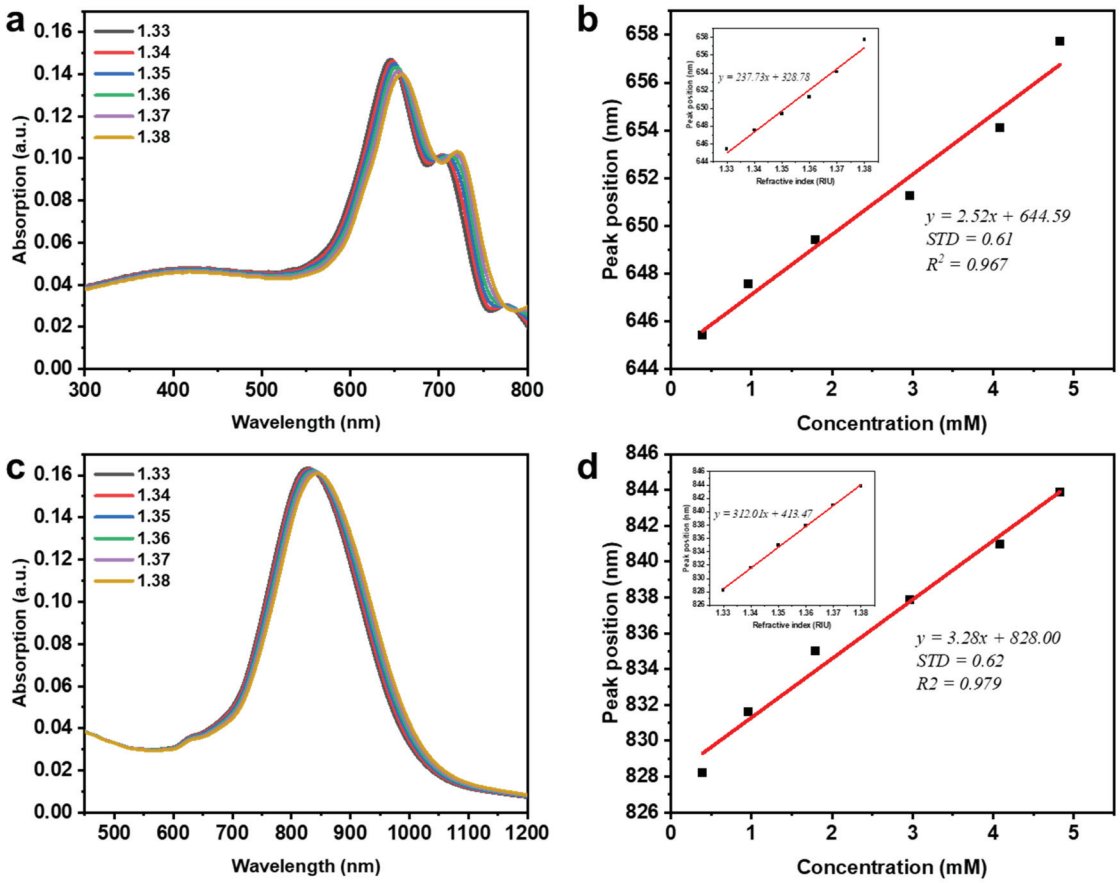

Figure 5. LSPR absorption response to refractive index change from 1.33 to 1.38. The linear plot shows the dependence on both concentration and refractive index (see inset). The refractive index change corresponds to the albumin concentration given in Table 1. The results show the comparison between bare hexaAu (a, b) and the silica-coated hexaAu (Si@hexaAu) (c, d).

Acknowledgement

This research received financial support from the Directorate of Higher Education, Ministry of Education and Culture, Republic of Indonesia (Grant Number: 1134/UN40.LP/PT.01.03/2024)

References

1. D. A. Belinskaia, P. A. Voronina, and N. V Goncharov, "Integrative role of albumin: evolutionary, biochemical and pathophysiological aspects," *J. Evol. Biochem. Physiol.*, vol. 57, no. 6, pp. 1419–1448, 2021.
2. C. Wang and L. A. Greenbaum, "Nephrotic syndrome," *Pediatric Clinics*, vol. 66, no. 1, pp. 73–85, 2019.
3. F. C. Alves *et al.*, "The higher mortality associated with low serum albumin is dependent on systemic inflammation in end-stage kidney disease," *PLoS One*, vol. 13, no. 1, p. e0190410, 2018.
4. C. P. Kovesdy, "Epidemiology of chronic kidney disease: an update 2022," *Kidney Int. Suppl. (2011).*, vol. 12, no. 1, pp. 7–11, 2022.
5. D. Kumar and D. Banerjee, "Methods of albumin estimation in clinical biochemistry: Past, present, and future," *Clinica Chimica Acta*, vol. 469, pp. 150–160, 2017.
6. R.-J. Yang, C.-C. Tseng, W.-J. Ju, H.-L. Wang, and L.-M. Fu, "A rapid paper-based detection system for determination of human serum albumin concentration," *Chemical Engineering Journal*, vol. 352, pp. 241–246, 2018.
7. M. Jamil *et al.*, "Quantitative determination of creatinine from serum of prostate cancer patients by N-doped porous carbon antimony (Sb/NPC) nanoparticles," *Bioelectrochemistry*, vol. 140, p. 107815, 2021.
8. H. S. Rafiq *et al.*, "Selective electrochemical sensing of hemoglobin from blood of β-thalassemia major patients by tellurium nanowires-graphene oxide modified electrode," *Chemical Engineering Journal*, vol. 419, p. 129706, 2021.
9. S. Palani *et al.*, "Multispectral localized surface plasmon resonance (msLSPR) reveals and overcomes spectral and sensing heterogeneities of single gold nanoparticles," *ACS Nano*, vol. 17, no. 3, pp. 2266–2278, 2023.

10. M. P. Raphael, J. A. Christodoulides, J. B. Delehanty, J. P. Long, P. E. Pehrsson, and J. M. Byers, "Quantitative LSPR imaging for biosensing with single nanostructure resolution," *Biophys. J.*, vol. 104, no. 1, pp. 30–36, 2013.
11. Z. Lin *et al.*, "On the role of localized surface plasmon resonance in UV-Vis light irradiated Au/TiO 2 photocatalysis systems: Pros and cons," *Nanoscale*, vol. 7, no. 9, pp. 4114–4123, 2015.
12. P. Yu, Y. Yao, J. Wu, X. Niu, A. L. Rogach, and Z. Wang, "Effects of plasmonic metal core-dielectric shell nanoparticles on the broadband light absorption enhancement in thin film solar cells," *Sci. Rep.*, vol. 7, no. 1, p. 7696, 2017.
13. K. Ai, J. Huang, Z. Xiao, Y. Yang, Y. Bai, and J. Peng, "Localized surface plasmon resonance properties and biomedical applications of copper selenide nanomaterials," *Mater. Today Chem.*, vol. 20, p. 100402, 2021.
14. P. Ravindra, "Protein-mediated synthesis of gold nanoparticles," *Materials Science and Engineering: B*, vol. 163, no. 2, pp. 93–98, 2009.
15. M. Shabaninezhad and G. Ramakrishna, "Theoretical investigation of size, shape, and aspect ratio effect on the LSPR sensitivity of hollow-gold nanoshells," *J. Chem. Phys.*, vol. 150, no. 14, 2019.
16. H. Zhang, X. Zhou, X. Li, P. Gong, Y. Zhang, and Y. Zhao, "Recent advancements of LSPR fiber-optic biosensing: Combination methods, structure, and prospects," *Biosensors (Basel).*, vol. 13, no. 3, p. 405, 2023.
17. H. Yin *et al.*, "Plasmonic and sensing properties of vertically oriented hexagonal gold nanoplates," *Nanoscale*, vol. 10, no. 31, pp. 15058–15070, 2018.
18. J. C. Martínez, A. K. Zavala, V. H. Romero, M. J. Yacamán, E. De la Rosa, and G. Plascencia, "Synthesis and characterization of gold star-shaped nanoparticles for biomedical applications," in *Latin America Optics and Photonics Conference*, Optica Publishing Group, 2014, pp. LTh4A-26.
19. S. S. Verma and J. S. Sekhon, "Influence of aspect ratio and surrounding medium on localized surface plasmon resonance (LSPR) of gold nanorod," *Journal of Optics*, vol. 41, pp. 89–93, 2012.
20. H. Yockell-Lelièvre, F. Lussier, and J.-F. Masson, "Influence of the particle shape and density of self-assembled gold nanoparticle sensors on LSPR and SERS," *The Journal of Physical Chemistry C*, vol. 119, no. 51, pp. 28577–28585, 2015.
21. G. Park *et al.*, "Strain-Induced Modulation of Localized Surface Plasmon Resonance in Ultrathin Hexagonal Gold Nanoplates," *Advanced Materials*, vol. 33, no. 38, p. 2100653, 2021.
22. W. A. Arcos Rosero, A. Bueno Barbezan, C. Daruich de Souza, and M. E. Chuery Martins Rostelato, "Review of Advances in Coating and Functionalization of Gold Nanoparticles: From Theory to Biomedical Application," *Pharmaceutics*, vol. 16, no. 2, p. 255, 2024.
23. C. Hanske, M. N. Sanz-Ortiz, and L. M. Liz-Marzán, "Silica-coated plasmonic metal nanoparticles in action," *Colloidal synthesis of plasmonic nanometals*, pp. 755–820, 2020.
24. V. Pellas *et al.*, "Gold Nanorod Coating with Silica Shells Having Controlled Thickness and Oriented Porosity: Tailoring the Shells for Biosensing," *ACS Appl. Nano Mater.*, vol. 4, no. 9, pp. 9842–9854, 2021.
25. H.-W. Han, A. Joe, and E.-S. Jang, "Reduced cytotoxicity of CTAB-templated silica layer on gold nanorod using fluorescence dyes and its application in cancer theranostics," *Journal of Industrial and Engineering Chemistry*, vol. 96, pp. 202–212, 2021.
26. L. Song *et al.*, "Amplifying the signal of localized surface plasmon resonance sensing for the sensitive detection of Escherichia coli O157: H7," *Sci. Rep.*, vol. 7, no. 1, p. 3288, 2017.
27. Q. Duan, Y. Liu, S. Chang, H. Chen, and J. Chen, "Surface plasmonic sensors: Sensing mechanism and recent applications," *Sensors*, vol. 21, no. 16, p. 5262, 2021.
28. C. Wulandari *et al.*, "Surface plasmon resonance biosensor chips integrated with MoS 2–MoO 3 hybrid microflowers for rapid CFP-10 tuberculosis detection," *J. Mater. Chem. B*, vol. 11, no. 48, pp. 11588–11599, 2023.
29. B. Archambeault, C. Brench, and O. M. Ramahi, "The Finite-Difference Time-Domain Method BT - EMI/EMC Computational Modeling Handbook," B. Archambeault, C. Brench, and O. M. Ramahi, Eds., Boston, MA: Springer US, 2001, pp. 35–70. doi: 10.1007/978-1-4615-1557-9_3.
30. J.-P. Berenger, "A perfectly matched layer for the absorption of electromagnetic waves," *J. Comput. Phys.*, vol. 114, no. 2, pp. 185–200, 1994, doi: https://doi.org/10.1006/jcph.1994.1159.
31. S. Ketrat, D. Japrung, and P. Pongprayoon, "Exploring how structural and dynamic properties of bovine and canine serum albumins differ from human serum albumin," *J. Mol. Graph. Model.*, vol. 98, p. 107601, 2020.
32. D. Shajari, A. Bahari, and P. Gill, "Fast and simple detection of bovine serum albumin concentration by studying its interaction with gold nanorods," *Colloids Surf. A Physicochem. Eng. Asp.*, vol. 543, pp. 118–125, 2018.

33. R. Barer and S. Tkaczyk, "Refractive index of concentrated protein solutions," *Nature*, vol. 173, no. 4409, pp. 821–822, 1954.
34. A. Muslihati *et al.*, "High-performance electrochemical biosensor comprising Mn-ZIF-67 conjugated with anti-O antibody for Escherichia coli detection," *Commun. Chem.*, vol. 8, no. 1, Dec. 2025, doi: 10.1038/s42004-025-01703-y.
35. Y. Huang, W. Wang, H. Liang, and H. Xu, "Surfactant-promoted reductive synthesis of shape-controlled gold nanostructures," *Cryst. Growth Des.*, vol. 9, no. 2, pp. 858–862, 2009.
36. M. Morsin, M. Mat Salleh, A. Ali Umar, and M. Z. Sahdan, "Gold Nanoplates for a Localized Surface Plasmon Resonance-Based Boric Acid Sensor," 2017. doi: 10.3390/s17050947.
37. J. E. Millstone, S. Park, K. L. Shuford, L. Qin, G. C. Schatz, and C. A. Mirkin, "Observation of a quadrupole plasmon mode for a colloidal solution of gold nanoprisms," *J. Am. Chem. Soc.*, vol. 127, no. 15, pp. 5312–5313, 2005.
38. X. Y. Gu, P. F. Gao, H. Y. Zou, J. H. Liu, Y. F. Li, and C. Z. Huang, "The localized surface plasmon resonance induced edge effect of gold regular hexagonal nanoplates for reaction progress monitoring," *Chemical Communications*, vol. 54, no. 95, pp. 13359–13362, 2018.
39. X. Xu *et al.*, "The influence of edge and corner evolution on plasmon properties and resonant edge effect in gold nanoplatelets," *Physical Chemistry Chemical Physics*, vol. 17, no. 4, pp. 2641–2650, 2015.
40. R. C. Monreal, T. J. Antosiewicz, and S. P. Apell, "Competition between surface screening and size quantization for surface plasmons in nanoparticles," *New J. Phys.*, vol. 15, no. 8, p. 83044, 2013.
41. Y. Fan, J. Li, H. Chen, X. Lu, and X. Liu, "Size-dependence of the effective electron-phonon energy relaxation in hollow gold nanospheres," *Opto-Electronics Review*, vol. 22, pp. 36–40, 2014.
42. R. Carmina Monreal, S. Peter Apell, and T. J. Antosiewicz, "Surface scattering contribution to the plasmon width in embedded Ag nanospheres," *Opt. Express*, vol. 22, no. 21, p. 24994, 2014, doi: 10.1364/oe.22.024994.
43. H. Baida *et al.*, "Quantitative determination of the size dependence of surface plasmon resonance damping in single Ag@ SiO2 nanoparticles," *Nano Lett.*, vol. 9, no. 10, pp. 3463–3469, 2009.
44. U. Guler and R. Turan, "Effect of particle properties and light polarization on the plasmonic resonances in metallic nanoparticles," *Opt. Express*, vol. 18, no. 16, pp. 17322–17338, 2010.
45. E. A. Coronado, E. R. Encina, and F. D. Stefani, "Optical properties of metallic nanoparticles: manipulating light, heat and forces at the nanoscale," *Nanoscale*, vol. 3, no. 10, pp. 4042–4059, 2011.
46. J. M. Zook, V. Rastogi, R. I. MacCuspie, A. M. Keene, and J. Fagan, "Measuring agglomerate size distribution and dependence of localized surface plasmon resonance absorbance on gold nanoparticle agglomerate size using analytical ultracentrifugation," *ACS Nano*, vol. 5, no. 10, pp. 8070–8079, 2011.
47. A. Candreva, W. Lewandowski, and M. La Deda, "Thickness control of the silica shell: a way to tune the plasmonic properties of isolated and assembled gold nanorods," *Journal of Nanoparticle Research*, vol. 24, no. 2, p. 19, 2022.
48. Z. Zhao *et al.*, "Thickness control of mesoporous silica coated on gold nanorod," *Journal of Nanoparticle Research*, vol. 23, pp. 1–12, 2021.
49. B. Grześkiewicz, K. Ptaszyński, and M. Kotkowiak, "Near and far-field properties of nanoprisms with rounded edges," *Plasmonics*, vol. 9, no. 3, pp. 607–614, 2014.
50. A. Candreva, W. Lewandowski, and M. La Deda, "Thickness control of the silica shell: a way to tune the plasmonic properties of isolated and assembled gold nanorods," *Journal of Nanoparticle Research*, vol. 24, no. 2, p. 19, 2022.
51. K. L. Kelly, E. Coronado, L. L. Zhao, and G. C. Schatz, "The optical properties of metal nanoparticles: the influence of size, shape, and dielectric environment," 2003, *ACS Publications*.
52. L. Rassinfosse, J. Müller, O. Deparis, S. Smeets, G. Rosolen, and S. Lucas, "Convergence and accuracy of FDTD modelling for periodic plasmonic systems," *Optics Continuum*, vol. 3, no. 6, pp. 844–858, 2024.
53. J. Wei, Z. Zeng, and Y. Lin, "Localized surface plasmon resonance (lspr)-coupled fiber-optic nanoprobe for the detection of protein biomarkers," *Biosensors and Biodetection: Methods and Protocols Volume 1: Optical-Based Detectors*, pp. 1–14, 2017.
54. A. Rabbani, R. Rudacille, and K. Hasegawa, "Local Refractive Index Sensitivity of Localized Surface Plasmon Resonance Biosensors," *The Journal of Physical Chemistry C*, 2024.
55. R. M. Sarimov, T. A. Matveyeva, A. L. Vasin, and V. N. Binhi, "Changes in the refractive index of a solution during proteolysis of bovine serum albumin with pepsin," *Biophysics (Oxf).*, vol. 62, no. 2, pp. 177–181, 2017, doi: 10.1134/S0006350917020221.